Submitted to ADVANCED MATERIALS

Supporting Information

for *Adv. Mater.*, DOI: 10.1002/adma.201604424

Exciton Diffusion Length and Charge Extraction Yield in Organic Bilayer Solar Cells

Bernhard Siegmund, Muhammad T. Sajjad, Johannes Widmer, Debdutta Ray, Christian Koerner, Moritz Riede, Karl Leo, Ifor D. W. Samuel*, Koen Vandewal**

Table of contents

SI.1 Literature: Previous exciton diffusion studies for ZnPc
SI.2 Overview of determination techniques
SI.3 Efficient exciton quenchers
SI.4 Exciton generation profile: Coverage of parabola approximation
SI.5 Boundary condition: Interface between absorber and transport layer
SI.6 Photo-current modelling: Analytical expression
SI.7 Photo-current modelling: Analysis of set 2
SI.8 Potential estimation: Conclusions for blended absorbers from diffusion study
SI.9 Time resolved photoluminescence: Details and evaluation guidelines
SI.10 References

SI.1 Literature: Previous exciton diffusion studies for ZnPc

Year	ℓ_d [nm]	η_c	Varying	Assuming ZnPc excitons reaching …	Modelled optics	… times sublimed	Layer sequence
1992 [1]	70	0.83	λ	Au to quench	Exp. decay	0?	Au|ZnPc|Au ?
1999 [2]	30	?	x_o	Hg to reflect	Exp. decay	0	ITO|PTCDI|ZnPc|Hg
2000 [3]	5	1.00 *	λ	Au to reflect	Interference	≥1	ITO|MPP|ZnPc|Au
2007 [4]	15	0.33	λ	ITO to reflect	Interference	>2	ITO|ZnPc|C60|BCP|Ag
2009 [5]	6	1.00 *	λ	ITO to reflect	Interference	≥1	ITO|ZnPc|PTCBI|BCP|Ag
2012 [6]	9	0.77	λ	?	Interference	0?	ITO|PEDOT:PSS|ZnPc|C60|?|Al

Table S1. Literature overview of previous measurements of ℓ_d in ZnPc based on photo-current modelling in chronological order. A star in the entry of the charge extraction yield assigns the respective value as input value for modelling. Otherwise, η_c was fitted along with ℓ_d from the experiment.

Table S1 gives an overview of previous exciton studies for ZnPc based on photo-current modelling including processing conditions and modelling details. While in general both the (i) absorber morphology and (ii) purity may effect the diffusion behaviour, we choose with ZnPc an absorber with negligible dependence for the specified parameters: (i) Schünemann *et al.* could demonstrate that ZnPc grows independent of the applied sublayer, both organic or inorganic, in the same crystalline phase, whereas X-ray diffraction (XRD) measurements suggest either triclinic (α-ZnPc) or monoclinic (γ-ZnPc) growth.[7] (ii) Moreover, Kerp *et al.* varied within their diffusion study the number of sublimation steps before device fabrication.[2] They report for ZnPc again only a negligible effect which might indicate an intrinsically high trap density that therefore can not be reduced by thermal vacuum sublimation. Finally, we neglect variations of the determined diffusion lengths in ZnPc due to processing conditions and focus on the modelling approach instead. For instance, exciton diffusion studies on ZnPc published before the year 2000 report overestimated diffusion lengths due to a drastically underestimated optical field, as a result of an inappropriate modelling technique. In a similar manner, also incorrectly modelled boundary conditions for exciton densities, rates of Förster transfer and/or exciton-exciton-annihilation may easily result over- or underestimations of ℓ_d by 100%.

SI.2 Overview of determination techniques

SI.2a Exciton diffusion length

In the following, the most common experimental techniques to determine ℓ_d are briefly discussed:

- **Photoluminescence quenching.** The first known approach[8] to determine ℓ_d exploits variations of the boundary conditions for an exciton distribution created upon absorption. Accordingly, inserting exciton quenching interfaces reduces both the emission intensity and exciton lifetime.[9,10] Hereby, a pronounced quenching effect

reflects a long-ranging exciton migration. Such techniques offer the advantage that the diffusion coefficient (time-resolved study) or length (steady-state study) typically represents the sole fitting parameter.[10,11] On the other hand, this approach requires semiconductors with some photoluminescence quantum yield.

- **Exciton-exciton-annihilation.** Instead of varying the layer thicknesses or area of quenching sites, as performed in the previous approach, here, the probability of exciton-exciton-annihilation is tuned by changing the excitation intensity over several orders of magnitude.[10,12] The advantage of evaluating only one sample is in opposition to the necessity of high photochemical stability and knowledge about the annihilation radius which is difficult to determine independently.
- **Time resolved microwave conductivity.** In contrast to the previous techniques, exciton diffusion can also be characterised by reading out a change in reflection in the microwave regime upon photo-excitation.[13] Hereby, the creation of excitons in an organic absorber is followed by exciton diffusion and splitting at an interface with TiO_2 leading to an injection of electrons into the latter. The resulting effect on the microwave reflectivity finally scales with the previous exciton diffusivity. Accordingly, such studies can be performed contact- and electrode-free. On the other hand, this type of study requires a sophisticated, non-standard characterisation setup.
- **Device modelling.** Whereas the previous techniques study thin-films, ℓ_d can also be extracted from modelling the output of opto-electronic organic devices, e.g. the photocurrent of solar cells[14] or the electroluminescence of light emitting diodes[15]. In this framework, the necessity to include the dynamics of charge extraction or injection into the modelling makes it more complex, but yields valuable insights into each device operation step under realistic conditions.

For all techniques, awareness for the correct Förster transfer rates and boundary conditions is required.[16] Moreover, a result has to be interpreted carefully when including effects which go beyond typical modelling, such as delocalisation or quenching grain boundaries.[17]

SI.2b Charge extraction yield

Assuming the absence of geminate recombination while splitting of the CT-state, η_c can be quickly estimated via a slope analysis of $j_{photo}(V)$ of a solar cell under reverse bias, whereas a fully saturated current for external voltages $V \leq 0$ indicates $\eta_c = 1$.[6,18,19] Unfortunately, bilayer solar cells rarely show the required saturation behaviour justifying this simplification. A further approach to determine η_c is restricted to devices with a blended photo-active system[20]. Moreover, for known exciton dynamics, both steady-state and transient[21] measurements of j_{photo} seem a reasonable choice to access η_c via Equation 1 in the main paper. In addition, also quantum-chemical[22] or dynamic Monte-Carlo[23] based simulations allow predictions on η_c.

SI.3 Efficient exciton quenchers

SI.3a High band gap alternatives to C_{60}

In order to allow a robust measurement with reasonable effort, we suggest transport (matrix) materials as exciton quenchers, as they ensure smoothly growing layers and high band gaps, thereby avoiding Förster transfer from the absorber to the quencher. Thus, when analysing a donor material, naphthalene diimides[24,25] or metal oxides as TiO_2[10] are often suitable. For accepting absorbers, diamines[26] or metal oxides as MoO_3[27] can be used.

SI.3b ZnPc-C_{60} cells: Choice of wavelength range for modelling

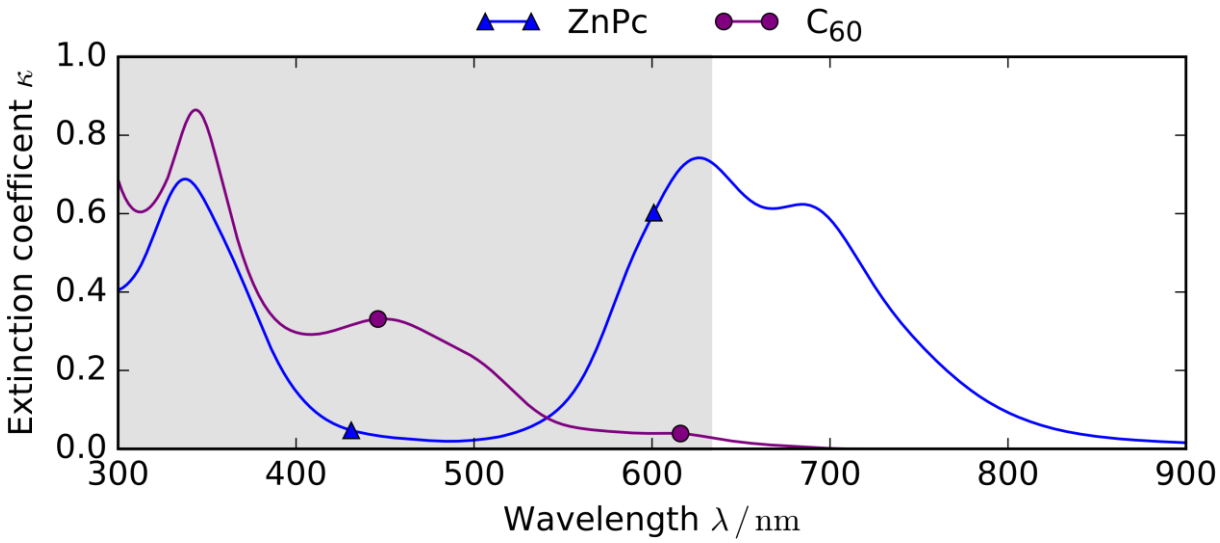

Figure S1. Comparison of extinction coefficients of the used absorbers. All excitation wavelengths applied to the solar cells address in ZnPc the Q-band which absorbs between 550nm and 800nm. Due to its smaller bandgap, ZnPc features dominant absorption for wavelengths exceeding 635nm (background highlighted). As performed for set 1 and 2, analysing this range allows neglecting photo-current originating from C_{60} absorption.

SI.4 Exciton generation profile: Coverage of parabola approximation

In order to quantify the deviation δ of the parabola approximated optical field $a_\lambda x^2 + b_\lambda x + c_\lambda$ from the simulated, $G(x)$, we define

$$\delta = \frac{\int_{ZnPc} \left| G(x) - \left(a_\lambda x^2 + b_\lambda x + c_\lambda\right) \right| dx}{\int_{ZnPc} G(x)\, dx} \qquad \text{(S0)}$$

As shown in Figure S2, δ does not exceed 3% for layer thicknesses of ZnPc of up to 100nm for both solar cell sets 1 and 2, which satisfies by far the requirements of the outlined method. When considering shorter wavelengths, the threshold thickness should decrease.

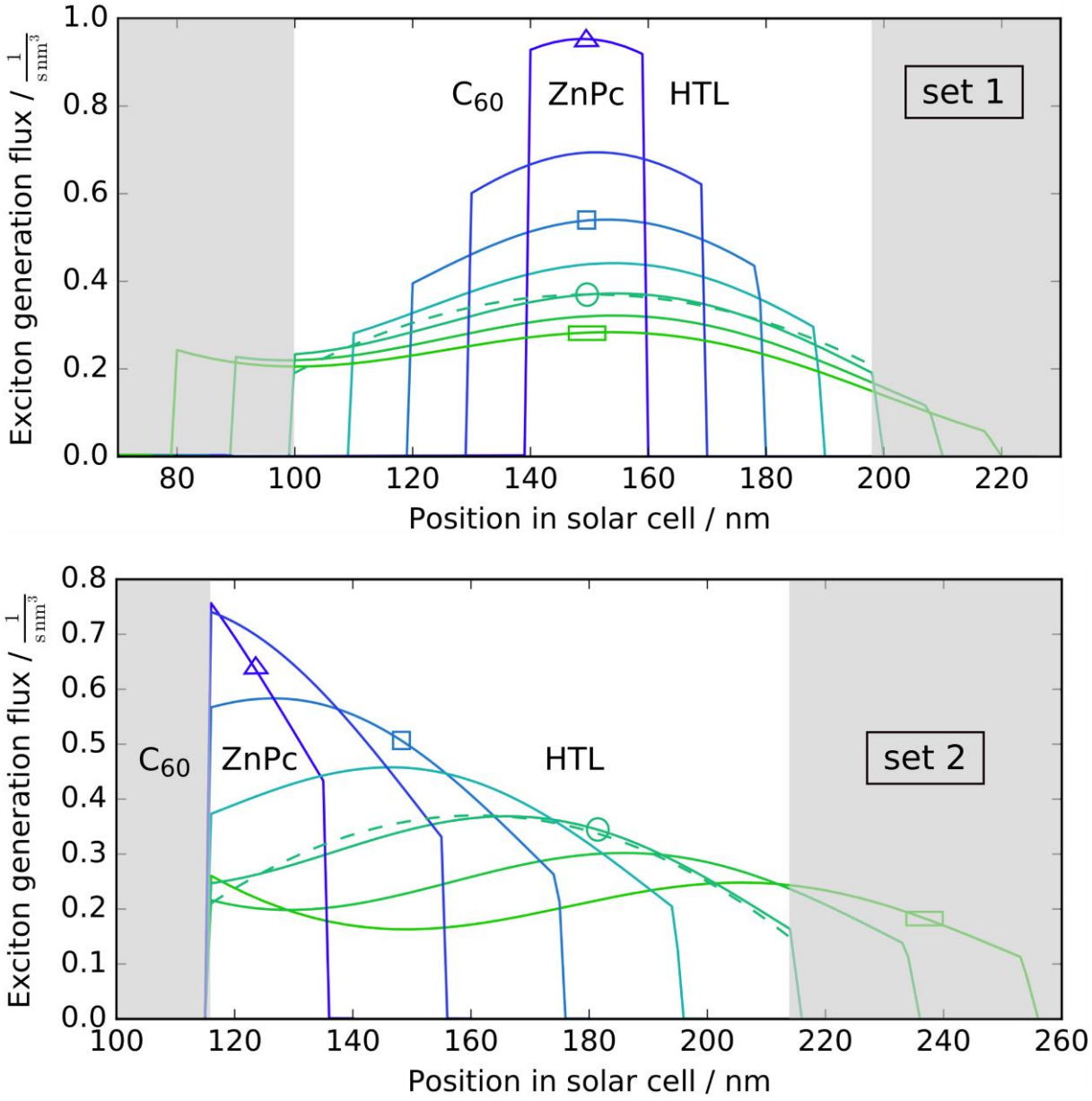

Figure S2. Simulated distribution of exciton generation flux (solid lines) in the solar cells of set 1 (top) and set 2 (bottom) when excited with a wavelength of 700nm. In comparison to Figure 1 in the main paper, also fictive samples with x_o up to 140nm layer thickness are simulated. For better readability, the following layer thicknesses are highlighted: 20nm (Δ), 60nm (□), 100nm (○), and 140nm (▭). For $x_o \leq 100$nm (highlighted by a white background), the deviation δ does not exceed 3%. For the limit case of x_o = 100nm, the respective approximating parabola is drawn as dashed line.

Moreover, the parabolic approximation of the optical field also holds for multiple flat heterojunctions (cascade cells) as well as bulk heterojunctions of comparable layer thickness, as *blended* absorbers exhibit similar optical constants to *neat* ones.

SI.5 Boundary condition: Interface between absorber and transport layer

When excitons generated in a donor-type absorber (optical gap of ZnPc: 1.5eV) reach the interface to a high bandgap material like the matrix of a doped transport layer (e.g. BF-DPB: 3.0eV and MeO-TPD: 2.9eV) they are reflected [28,29], unless they split due to a high HOMO or LUMO-offset (as the case for the C_{60} interface). Due to the alignment of the HOMO energies, we expect complete reflection of ZnPc excitons reaching the intrinsic MeO-TPD. The same reasoning holds for the interface with BF-DPB neglecting the presence of 10wt% dopant.

SI.6 Photo-current modelling: Analytical expression

SI.6a Derivation of analytical expression

The photo-current originates from the flux of excitons diffusing from an absorption site in the donor (i=D) or acceptor (i=A) to their joint interface (D|A):

$$j_{photo} = e_c \eta_c (x_o) \sum_{i=D,A} D^i \left| \frac{\partial n^i_{D|A}}{\partial x} \left(x^i_o, G^i, \ell^i_d, k^i_F, \alpha^i, BC^i \right) \right| \qquad \text{(S1)}$$

whereas η_c represents the combined efficiency of CT state splitting and subsequent extraction of the charges at the designated electrode.[14] Thus, besides charge extraction, j_{photo} strongly depends on the spatial distribution of excitons in both absorbers. The latter in turn is also a function of the distribution of optical field, as well as diffusion lengths, rates of Förster transfer and exciton-exciton-annihilation ruling in both photo-active layers.

In earlier studies where bilayer solar cells with thin absorber layers were considered, the optical field within one absorber was simplified as constant: $G^i(x) \approx G_o^i$. In this *most simple case* (furthermore $\alpha = 0, k^A_{FRET} = k^{HTL}_{FRET} = 0$), the photo-current can be expressed as

$$j_{photo} \approx e_c \eta_c (x_o) \sum_{i=D,A} G^i_o \ell^i_d \tanh\left(f^i_{BC} x^i_o / \ell^i_d \right) \qquad \text{(S2)}$$

where $f_{BC} \in [0.5,1]$ denotes a prefactor[19] attributed to the chosen boundary conditions.

In the following, we show how to extend the analytical expression for j_{photo} when considering more realistic scenarios for the distribution of the optical field in solar cells. For this purpose, we solve the differential equation for exciton dynamics, as introduced in the main paper

$$\frac{\partial n}{\partial t} = D\frac{\partial^2 n}{\partial x^2} + G(x,t) - k_{PL}(t)\cdot n - k_{FRET}(x)\cdot n - \alpha\cdot n^2 \tag{S3}$$

where we consider only low energy photons with exclusive donor absorption (G^A=0) and thus drop the layer index for the donor (i=D) for better readability.

Multiple simplifications (as in the main paper)

$$\frac{\partial n}{\partial t} = 0, k_{PL} = 1/\tau_o = D/\ell_d^2, \alpha = 0, k_{FRET}^A = k_{FRET}^{HTL} = 0 \tag{S4}$$

lead to the steady-state equation

$$G(x) = D\left(\frac{1}{\ell_d^2} - \frac{\partial^2}{\partial x^2}\right)n \tag{S5}$$

As calculated by Yoo *et al.*,[30]

$$Dn(x) = \left[k_1 - \frac{\ell_d}{2}\int_{x_o}^{x} e^{-\hat{x}/\ell_d} G(\hat{x})d\hat{x}\right]e^{x/\ell_d} + \left[k_2 + \frac{\ell_d}{2}\int_{x_o}^{x} e^{\hat{x}/\ell_d} G(\hat{x})d\hat{x}\right]e^{-x/\ell_d} \tag{S6}$$

represents the general solution for Equation S5 for arbitrarily shaped excitation profiles G(x). For this work, we choose a parabolic excitation profile

$$G_\lambda(x) = a_\lambda x^2 + b_\lambda x + c_\lambda \quad \text{(S7)}$$

which is a good approximation within the framework of interference based thin-film optics, as demonstrated in SI.4.

We obtain the solution

$$Dn(x) = k_1 e^{x/\ell_d} + k_2 e^{-x/\ell_d} + \ell_d^2 \left[G_\lambda(x) + 2a_\lambda \ell_d^2 - \cosh\left(\frac{x-x_o}{\ell_d}\right)\beta(x_o) - \sinh\left(\frac{x-x_o}{\ell_d}\right)(2a_\lambda x_o \ell_d + b_\lambda \ell_d) \right] \quad \text{(S8)}$$

with

$$\beta(x_o) = G_\lambda(x_o) + b_\lambda x_o + 2a_\lambda \ell_d^2 \quad \text{(S9)}$$

Applying the boundary conditions of complete exciton quenching at the DA-interface (x=x_o) and complete exciton reflection at the donor-HTL interface (x=0, discussed in SI.5)

$$n(x = x_o) = 0 \wedge \frac{\partial n}{\partial x_o}(x = 0) = 0 \quad \text{(S10)}$$

the coefficients k_1 and k_2 can be determined, finally leading to the photo-current

$$j_{photo} = \ell_d \left[\tanh\frac{x_o}{\ell_d}\left(G_\lambda(x_o) + 2a_\lambda \ell_d^2\right) + b_\lambda \ell_d \left(1/\cosh\left(\frac{x_o}{\ell_d}\right) - 1 \right) - 2a_\lambda x_o \ell_d \right] e\eta_c \quad \text{(S11)}$$

where all orders of the optical field are now coupled to exciton diffusion. Furthermore, it may be mentioned that ZnPc exhibits the specific feature of exciton dissociation upon reaching a crystalline domain[31] within neat layers. As occurring only in small rates, it is neglected in our analysis.

SI.6b Discussion of the found expression

The found relation between the photocurrent, the solar cell geometry and materials constants, such as diffusion lengths and optical constants, as here derived for flat heterojunctions, may be extended to other architectures: (i) For cascade cells, the photocurrent is calculated as sum of currents generated in each photoactive layer. In contrast to cascades purely based on charge transfer, attention has to be paid when studying absorber combinations with non-negligible Förster transfer which implies non-analytical solutions for the photocurrent. (ii) Transferring the presented technique to characterise bulk heterojunctions is difficult since it would require a precise microscopic knowledge of the molecular blend, e.g. the 3-dimensional distribution function of all present domain sizes in the donor-acceptor-blend.

The interdiffusion of donor-C_{60}-bilayers can be suppressed by choosing donor materials with a high glass transition temperature,[32] as is the case for ZnPc with a glass transition at 240°C.[33] Moreover, the devices are processed without substrate heating or thermal annealing which are known to cause interdiffusion.[34,10] Although we do not expect any interdiffusion for our material system, the device modelling approach is in principle capable of accounting for it: We introduce an effective penetration depth of Fullerenes Δx into the donor which would cause, if unaccounted, an overestimated the diffusion length ℓ_d. When inserting the reduced donor thickness $\hat{x}_o$ into the photocurrent expression, we obtain the correct diffusion length $\hat{\ell}_d$:

$$j_{photo}(\hat{x}_o, \hat{\ell}_d) = j_{photo}(x_o - \Delta x, \hat{\ell}_d) \tag{S12}$$

SI.7 Photo-current modelling: Analysis of set 2

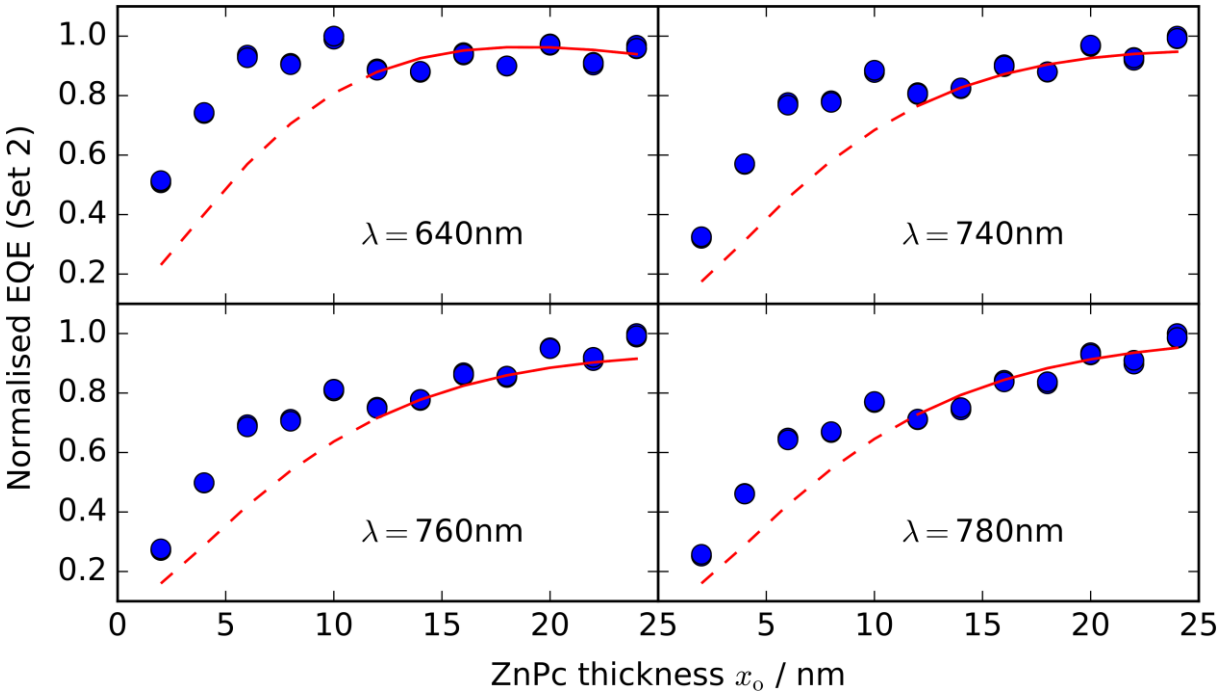

Figure S3. External quantum efficiency (EQE) of set 2 from Figure 1 in the main paper under variation of the layer thickness of ZnPc x_o and the excitation wavelength λ. The experimental data (circles) is jointly fitted (solid lines) for all x_o and λ according to Equation S11. The dashed lines indicate the prolongation of the fit for the range of samples ($x_o \leq$11nm) discarded due to layer roughness, interdiffusion and/or space charge build-up at the donor-acceptor-interface. The extracted diffusion length in ZnPc is ℓ_d =(10.2±0.8)nm and the charge extraction yield is η_c= (58±6)%. For better readability, the EQE is normalised to its experimental maximum of the respective sub-graph, namely to 10.1%, 6.0%, 4.4% and 2.7% (read for increasing wavelength).

SI.8 Potential estimation: Conclusions for blended absorbers from diffusion study

Studying flat heterojunction devices itself, as described in the framework of this exciton diffusion study, is also beneficial to estimate the potential of blended systems, as they

- allow valuable insights in charge losses due to recombination processes, which turn out as bottlenecks for all photovoltaic parameters (e.g. photo-current, fill-factor and open-circuit voltage), also in bulk heterojunction systems. Accordingly, if an absorber combination shows in a bilayer device pronounced losses in η_c, but yet a reasonable fill-factor, it can be discarded for further optimisation routines, due to harmful charge recombination at the DA-interface.

- provide a quantitative upper limit of the achievable open circuit voltage[35], due to suppressed bimolecular recombination arising from reduced donor-acceptor surface.
- provide a quantitative upper limit of the achievable fill-factor, as neat layers typically exhibit higher mobilities and thus enhanced charge transport.
- give hints on optimum processing conditions for blended absorber systems, as known diffusion lengths imply a maximum suitable domain size in absorber blends. Thus, small diffusion lengths suggest fine-grained blends which means, for example in the context of small molecules, typically low substrate temperatures. Moreover, if the analysis of two blend constituents exhibits a strong asymmetry in exciton migration, it directly suggests an unbalanced blending ratio for an optimum generation of photo-current.

SI.9 Time resolved photoluminescence: Details and evaluation guidelines

The emission of ZnPc has its onset at around 750-800nm, as described in References [22] and [31]. The PL decays are recorded for wavelengths between 810nm and 830nm. The decay of a 100nm thick ZnPc thin-film on quartz glass (not shown) reads an intrinsic exciton lifetime of 2.9ns and a slightly accelerated PL decay within the first 150ps allowing to conclude a flat energetic landscape as typical[36] for small molecules.

For analysing the PL decays by means of Equation 2 in the main paper, we choose G=0 (i.e. no further excitation after an initial fs-laser-pulse) and α=0 (initial exciton population in the order of $<10^{15}$cm^{-3}). As FRET dynamics are included into the evaluation, the time dependent exciton distribution n is obtained by solving Equation 2 numerically in the presence and absence of the exciton quencher C_{60}. After spatial integration and division of both solutions, D is varied for the obtained function to fit the experimental PL quotient.

SI.10 References

[1] D. Meissner, S. Siebentritt, S. Günster, *Int. Soc. Opt. Eng.* **1992**, *1729*, 24.

[2] H. R. Kerp, E. E. van Faassen, *Phys. Chem. Chem. Phys.* **1999**, *1*, 1761.

[3] J. Rostalski, D. Meissner, *Sol. Energy Mater. Sol. Cells* **2000**, *63*, 37.

[4] Y. Terao, H. Sasabe, C. Adachi, *Appl. Phys. Lett.* **2007**, *90*, 103515.

[5] I. Kim, H. M. Haverinen, Z. Wang, S. Madakuni, Y. Kim, J. Li, G. E. Jabbour, *Chem. Mater.* **2009**, *21*, 4256.

[6] J. Yang, F. Zhu, B. Yu, H. Wang, D. Yan, *Appl. Phys. Lett.* **2012**, *100*, 103305.

[7] C. Schünemann, C. Elschner, A. A. Levin, M. Levichkova, K. Leo, M. Riede, *Thin Solid Films* **2011**, *519*, 3939.

[8] O. Simpson, *Proc. R. Soc. A* **1957**, *238*, 402.

[9] A. K. Topczak, T. Roller, B. Engels, W. Brütting, J. Pflaum, *Phys. Rev. B* **2014**, *89*, 1.

[10] P. E. Shaw, A. Ruseckas, I. D. W. Samuel, *Adv. Mater.* **2008**, *20*, 3516.

[11] O. V Mikhnenko, F. Cordella, A. B. Sieval, J. C. Hummelen, P. W. M. Blom, M. A. Loi, *J. Phys. Chem. B* **2009**, 9104.

[12] Z. Masri, A. Ruseckas, E. V. Emelianova, L. Wang, A. K. Bansal, A. Matheson, H. T. Lemke, M. M. Nielsen, H. Nguyen, O. Coulembier, P. Dubois, D. Beljonne, I. D. W. Samuel, *Adv. Energy Mater.* **2013**, *3*, 1445.

[13] J. E. Kroeze, T. J. Savenije, M. J. W. Vermeulen, J. M. Warman, *J. Phys. Chem. B* **2003**, *107*, 7696.

[14] A. K. Ghosh, T. Feng, *J. Appl. Phys.* **1978**, *49*, 5982.

[15] S. Hofmann, T. C. Rosenow, M. C. Gather, B. Lüssem, K. Leo, B. Lüssem, K. Leo, *Phys. Rev. B* **2012**, *85*, 245209.

[16] W. A. Luhman, R. J. Holmes, *Adv. Funct. Mater.* **2011**, *21*, 764.

[17] O. V. Mikhnenko, J. Lin, Y. Shu, J. E. Anthony, P. W. M. Blom, T.-Q. Nguyen, M. A. Loi, *Phys. Chem. Chem. Phys.* **2012**, *14*, 14196.

[18] J. Meiss, M. Hermenau, W. Tress, C. Schuenemann, F. Selzer, M. Hummert, J. Alex, G. Lackner, K. Leo, M. Riede, *Phys. Rev. B* **2011**, *83*, 1.

[19] C. Uhrich, Strategien Zur Optimierung Organischer Solarzellen, TU Dresden, *Dissertation*, **2008**.

[20] R. Pandey, R. J. Holmes, *Appl. Phys. Lett.* **2012**, *100*, 083303.

[21] T. K. Mullenbach, R. J. Holmes, *Appl. Phys. Lett.* **2015**, *107*, 123303.

[22] B. P. Rand, D. Cheyns, K. Vasseur, N. C. Giebink, S. Mothy, Y. Yi, V. Coropceanu, D. Beljonne, J. Cornil, J. L. Brédas, J. Genoe, *Adv. Funct. Mater.* **2012**, *22*, 2987.

[23] F. Yang, S. R. Forrest, *ACS Nano* **2008**, *2*, 1022.

[24] C. Falkenberg, K. Leo, M. K. Riede, *J. Appl. Phys.* **2011**, *110*, 124509.

[25] R. Meerheim, C. Körner, B. Oesen, K. Leo, *Appl. Phys. Lett.* **2016**, *108*, 103302.

[26] T. Menke, D. Ray, H. Kleemann, M. P. Hein, K. Leo, M. Riede, *Org. Electron.* **2014**, *15*, 365.

[27] H. Kanno, R. J. Holmes, Y. Sun, S. Kena-Cohen, S. R. Forrest, *Adv. Mater.* **2006**, *18*, 339.

[28] P. Peumans, A. Yakimov, S. R. Forrest, *J. Appl. Phys.* **2003**, *93*, 3693.

[29] M. Riede, T. Müller, W. Tress, R. Schüppel, K. Leo, *Nanotechnology* **2008**, *19*, 424001.

[30] S. Yoo, B. Domercq, B. Kippelen, *Appl. Phys. Lett.* **2004**, *85*, 5427.

[31] D. Ray, M. Furno, E. Siebert-Henze, K. Leo, M. Riede, *Phys. Rev. B* **2011**, *84*, 075214.

[32] J. J. M. Halls, K. Pichler, R. H. Friend, S. C. Moratti, A. B. Holmes, *Appl. Phys. Lett.* **1996**, *68*, 3120.

[33] G. A. Kumar, J. Thomas, N. George, N. V. Unnikrishnan, P. Radhakrishnan, V. P. N. Nampoori, C. P. G. Vallabhan, *J. Mater. Sci.* **2000**, *35*, 2539.

[34] D. E. Markov, E. Amsterdam, P. W. M. Blom, A. B. Sieval, J. C. Hummelen, *J. Phys. Chem. A* **2005**, *109*, 5266.

[35] K. Vandewal, S. Albrecht, E. T. Hoke, K. R. Graham, J. Widmer, J. D. Douglas, M. Schubert, W. R. Mateker, J. T. Bloking, G. F. Burkhard, A. Sellinger, J. M. J. Fréchet, A. Amassian, M. K. Riede, M. D. McGehee, D. Neher, A. Salleo, *Nat. Mater.* **2014**, *13*, 63.

[36] S. M. Menke, R. J. Holmes, *Energy Environ. Sci.* **2014**, *7*, 499.